Predictions and Magnetic Characterization of M-type Hexaferrites Doped with Two Cations in the Fe^{3+} Site

Pedro Antonio Mariño-Castellanos[1, *], Valery Alexevich Lapshinsky[2], Carlos Pupo[1, 2], Arles Vega-García[1], Eduardo Fernández-Cruz[3], Braddy Ivan Jimenez-Morales[4]

[1]University of Holguin, Holguin, Cuba

[2]Peoples Friendship University of Russia, Moscow, Russian Federation

[3]Department of Physics, University of Camagüey, Camagüey, Cuba

[4]Physics Institute, Kazan Federal University, Kazan, Russian Federation

Email address:
pamarcast@uho.edu.cu (P. A. Mariño-Castellanos)
[*]Corresponding author

To cite this article:

Abstract: A theoretical and experimental study of magnetic properties of M-type barium hexaferrites, doped with two cations in the Fe^{3+} sites: (Co^{3+}, Al^{3+}), (Co^{2+}, Ti^{4+}) and (Co^{2+}, Sn^{4+}) is reported. The theoretical predictions were made using the generalization of a model on the distribution of dopants in the crystallographic sites under study. This approach allows a better interpretation of the kinetics of obtaining the samples from the structural and magnetic characterization. In the reported model, the maximum limit refers to theoretical optimum parameters. With these concepts, were established quantitative relationships between dopant amount per crystallographic site and magnetic properties predicted of these systems. The comparison between the experimental values and the predicted magnitudes showed that, in general, the samples were obtained with parameters obtained close to the theoretical ones for traditional ceramic methods. Such an approach is rarely taken into account in the reported bibliography.

Keywords: Sol-Gel Methods, Magnetic Properties, Hexaferrite, Theoretical Predictions, Rietveld Refinement

1. Introduction

The magnetic structure of BaM is described by the Gorter model as an uniaxial collinear ferrite [1], with three spin-up (2a, 2b, 12k) and two spin-down (4fiv, 4fvi) sublattices along the c-axis. It is a ferromagnetic material with high coercitivity, magnetic permeability, saturation magnetization and magneto-crystalline anisotropy along the c-axis [2]. Its magnetic properties are functions of the crystalline microstructure [2, 3].

Several investigations have been carried out to study the influence of various dopants on its physical properties of M-type hexaferrites. The microstructural modification of the barium hexaferrite structure, leads to change in magnetic, and microwave properties, an effective method is the doping of Ba^{2+} or Fe^{3+} cations sites with other metallic cations. During the past few years it becomes possible to synthesize some substitution M-type hexaferrites in which coercivity decline effectively with cations dopant. To achieve this objective, we have, the doping of transition metals, e.g., Co^{2+}, Mg^{2+}, Zn^{2+}, Ni^{2+}, Al^{3+}, Cr^{3+}, Ti^{4+}, Zr^{4+}, and Sn^{4+}, which has been investigated by several researchers to modify different properties of M-type hexaferrite [4, 5].

However, only few theoretical studies about M-type hexaferrites have been reported regarding in relation with the cation distribution in the different crystallographic sites of this crystal structure [4, 6].

The objective of the present investigation is to establish the dependences on the microstructure of the magnetic properties of M-type barium hexaferrites doped with (Co^{3+}, Al^{3+}), (Co^{2+}, Ti^{4+}) and (Co^{2+}, Sn^{4+}) in the iron sites and their comparison with the theoretical predictions obtained of the

generalization of a model on the distribution of dopants in the crystallographic sites under study.

2. Materials and Methods

The samples were obtained by the traditional ceramic method, using $BaCO_3$, Fe_2O_3, Al_2O_3, TiO_2, CoO, Co_2O_3 and SnO_2 as starting materials. They were mixed in the required stoichiometric ratio according to the chemical formula $BaFe_{(12-2xDj)}A_{xDj}B_{xDj}O_{19}$ where $A_{xDj}=Al^{3+}$, Ti^{4+}, Sn^{4+} and $B_{xDj}=Co^{3+}$, Co^{2+}.

The structural characterization was carried out from the X rays diffraction patterns, and the wavelength of radiation was Co $[\lambda(k_{\alpha 1})] = 1.788\ 9$ Å.

The qualitative phase analysis was carried out by Hanawalt method and software Match Phase Identification from Powder Diffraction. Each diffraction pattern was refined by Rietveld method, using the Fullprof software [4, 6, 7].

The magnetic study were characterized by using of a rotating sample magnetometer (RSM) [4, 6, 7].

3. The Phenomenological Model

The total quantity of dopants in each site [4, 6] is expressed by the previous model in the following way:

$$C_{xDp,xDj}(i) = N(i) - C_C(xDp, xDj, i) \tag{1}$$

and the quantity of each dopant per site:

$$C_{xDp}(xDj, i) = C_{xDp,xDj}(i)PS_{xDp}(xDj, i) \tag{2}$$

$$C_{xDj}(xDp, i) = C_{xDp,xDj}(i)PS_{xDj}(xDp, i) \tag{3}$$

The expressions from (1) to (3) are similar to those used in [7] when data from Mössbauer spectrometry are interpreted for the case of doping with two dopants.

Until here, the results contributed by this model represent the values to obtain in the case of ideal substitutions with optimum obtaining parameters, which do not involve any obtaining method. However, when the dopant is included, the optimum obtaining parameters for un-doped hexaferrites are not the same that parameters for doped samples, and the magnitude of such variation depends on concentration and dopant type [4, 6], as it can be observed from the generalized Kapustinskii equation [8] for the energy, in function of each crystallographic site:

$$U_{rsite} = \frac{1214\,\gamma Z_C Z_a}{r_C + r_a}\left[\left(1 - \frac{34.5}{r_C + r_a}\right) + 0.00453(r_C + r_a)\right] [KJ/mol] \tag{4}$$

Where U_{rsite} - reticular energy per site; $[r]=10^{-12}$ m; γ - quantity of ions per formula unit; Z_c – cation atomic number; Z_a – anion atomic number; r_c – cationic radius and r_a - anionic radius.

The dependence on dopant type (through Z_c), quantity of dopant (through γ) and crystallographic sites (through r_c and r_a) are presented, theoretically demonstrating this dependence during the formation process of doped BaM [4, 9].

Equation (4) allows theoretical calculation of the involved formation energy in the sites where the dopants and the cations number are distributed, using the expressions (1), (2)

and (3). Then, the equations that explain the nucleation kinetics [10] are applied to calculate the nucleation energy parameters in each case DRxDj (xDp, i) and DRxDp (xDj, i).

The maximum and minimum limits of the cations distribution per sites can be reported:

$$C_{xDp}(xDj, i)_{max} = xDp\,\frac{g_{xDp}(xDj,i)}{g_{xDp}(xDj,i)+g_{xDj}(xDj,i)} \tag{5}$$

$$C_{xDj}(xDj, i)_{max} = xDj\,\frac{g_{xDj}(xDj,i)}{g_{xDp}(xDj,i)+g_{xDj}(xDj,i)} \tag{6}$$

$$C_C(xDp, xDj, i)_{min} = N(i) - \left[C_{xDp}(xDj, i)_{max} + C_{xDj}(xDj, i)_{max}\right] \tag{7}$$

$$C_{xDp}(xDj, i)_{min} = C_{xDp}(xDj, i)_{max}DR_{xDp}(xDj, i) \tag{8}$$

$$C_{xDj}(xDj, i)_{min} = C_{xDj}(xDj, i)_{max}DR_{xDj}(xDj, i) \tag{9}$$

$$C_C(xDp, xDj, i)_{max} = N(i) - \left[C_{xDp}(xDj, i)_{min} + C_{xDj}(xDj, i)_{min}\right] \tag{10}$$

The equations from (5) to (10) allow the calculation of substitutes cations distribution for optimum obtaining parameters (maximum values) and when these parameters change as a function of temperature and calcination time (minimum values) [10]. Therefore, it is possible to predict

the behavior of saturation magnetization MS, magneto-crystalline anisotropic constant K1 and coercitive field HC.

Assuming a collinear arrangement of the magnetic domains in the Fe3+ sites, the theoretical value of MS [6, 9, 11] can be calculated through the expression:

$$M_S = \mu_{Fe^{3+}(2a)} + \mu_{Fe^{3+}(2b)} - 2\mu_{Fe^{3+}(4fiv)} - 2\mu_{Fe^{3+}(4fiv)} + \mu_{Fe^{3+}(12k)} \tag{11}$$

Where $\mu_{Fe^{3+}}$ is the standard value of the Fe^{3+} magnetic moment, and since $\mu_{Fe^{3+}} = 5\mu_B$ at 0K (μ_B -Bohr's magneton) will exist a total MS=$20\mu_B$ per formula unit for

un-doped $BaFe_{12}O_{19}$ at this temperature. Extending the previous expression to the case of doped BaM with two dopants [4]:

$$M_S = \sum_{i=1}^{5}(CCS_i \cdot \mu_{Fe^{3+}} + CDS_iD_j \cdot \mu_{Dj} + CDS_iD_p \cdot \mu_{Dp}) \tag{12}$$

For the axial-c anisotropy, $K_1 > 0$ and, usually, K_2 is negligible in comparison with K_1. In this case, magneto-crystalline anisotropy field H_{an} [4, 12] is given by:

$$H_{an} = \frac{2K_1}{M_S} \qquad (13)$$

and anisotropy constant K_1 [4] is determined by:

$$K_1 = M_{perp}^{max} H \qquad (14)$$

Where M_{perp}^{max} is the maximum perpendicular magnetization, measured in the RSM and H is the field under which the previous value was obtained.
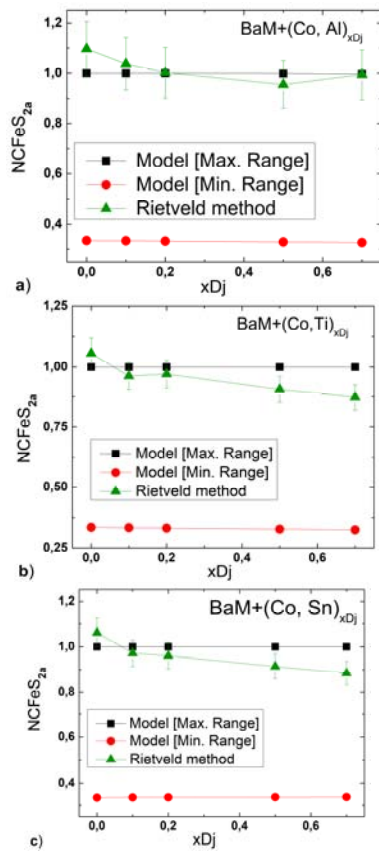
According to the Stoner-Wohlfarth theory [13], coercivity is given by

$$H_C = \alpha \left[\frac{2K_1}{M_S} - DM_S \right] \qquad (15)$$

Where α is a geometrical parameter (α = 0.48 in case of randomly oriented particles) and D is the demagnetization factor.

4. Results and Discussion

In the figures from 1 to 5 it is shown a comparison between cation's distributions experimentally determined and the predictions by the cation's distribution model, in the different Fe^{3+} sites.

In general, is observed a gradual decrease of the Fe^{3+} cation quantity in each site, whose dependence varies with the concentration and dopant type. The difference between maximum values of theoretical and experimental cation's distribution per site indicates that preparation parameters outdistance the optimum parameters. An abrupt change of this curve with $xDj \geq xDj_{critical}$ is noticed.
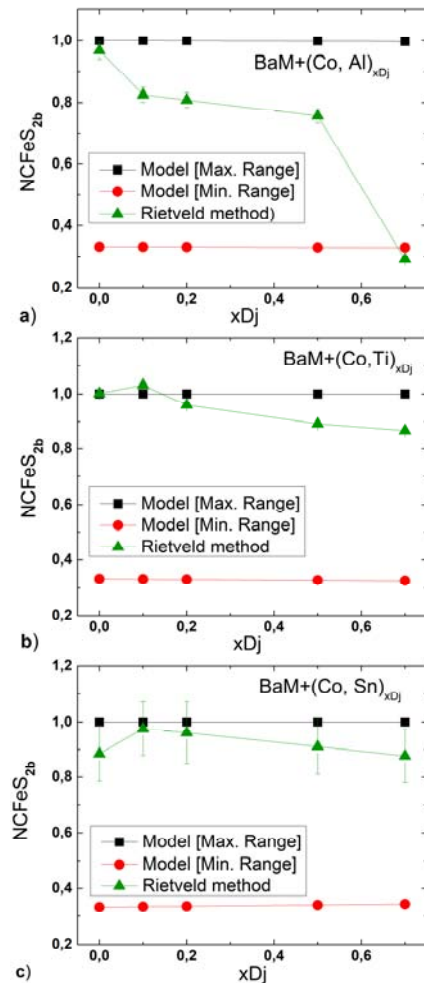
The minimum predicted values refer the increase or decrease of required energy for compound formation.

The dopants occupy the spaces that were left by Fe^{3+} in each crystallographic position, in function of the preferential site for each one [4, 6].

In the figure 1 it is evident that in the doping range where doped BaM phase is in majority, this site is not a preferential one for the dopants considered in this investigation.

In the figure 2 is evident that for BaM + $(Co, Al)_{xDj}$ the quantity of the ion Fe3+ decreases and it is not compensated by the dopant quantity that goes to this site.

For BaM+ $(Co, Ti)xDj$ there is not variation for the iron ion until xDj is near the $xDj_{critical}$. For BaM + $(Co, Sn)_{xDj}$ the quantity of iron remains approximately constant in the whole range where this phase is in majority.

Figure 1. *Comparison between the experimental results of the Fe^{3+} distribution determined by the Rietveld method and the predictions by the model for crystallographic site 2a, per formula unit.*
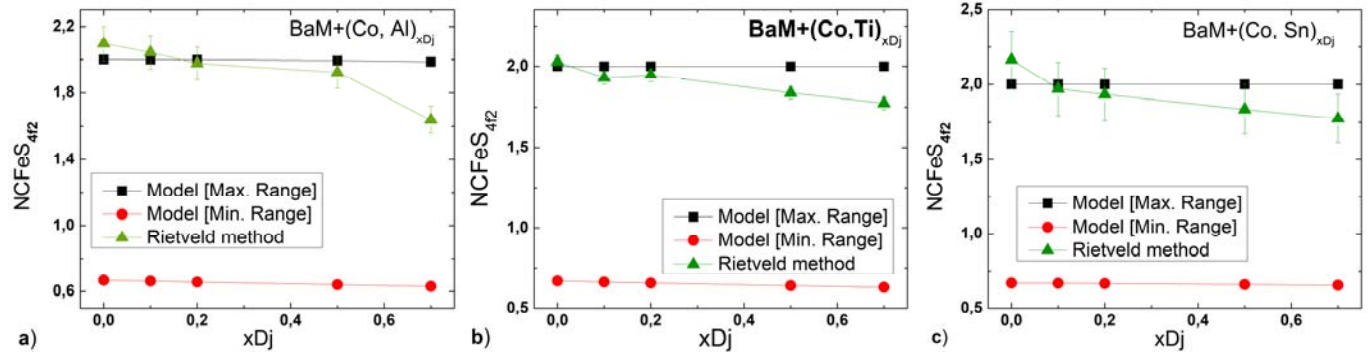

Figure 2. *Comparison between the experimental results of the Fe^{3+} distribution determined by the Rietveld method and the predictions by the model for crystallographic site 2b, per formula unit.*

In the figure 3, it can be appreciated that the decrease of the iron cation quantity in the site 4fiv is appreciable, but small, only starting from xDjcritical for BaM + (Co, Sn)xDj.
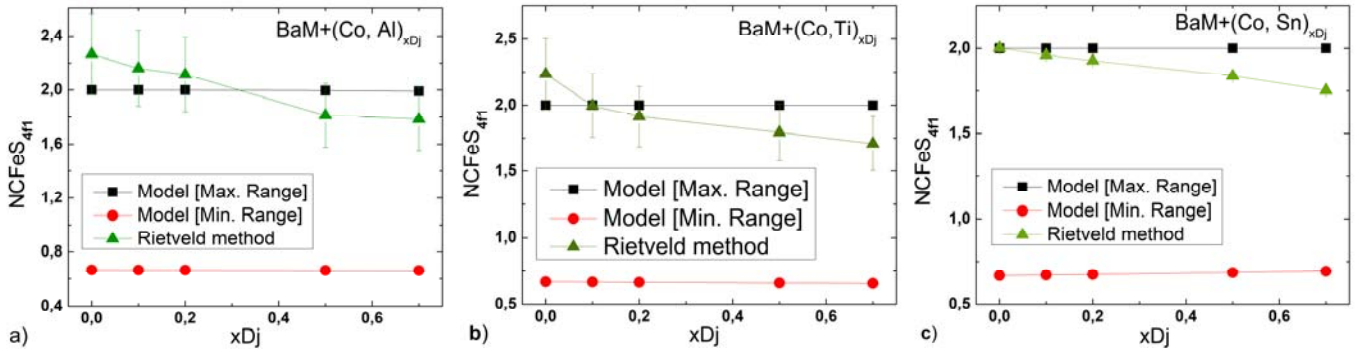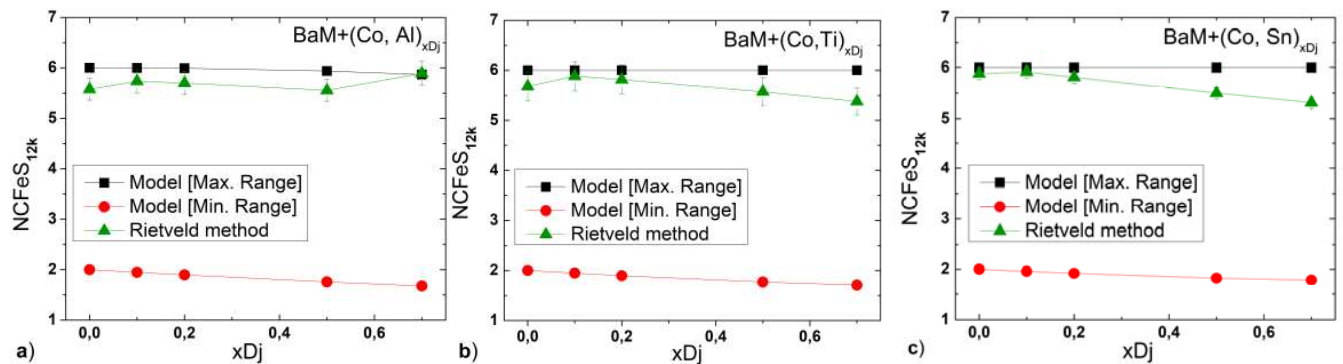

Figure 3. *Comparison between the experimental results of the Fe^{3+} distribution determined by the Rietveld method and the predictions by the model for crystallographic site 4fiv, per formula unit.*

The site 4fvi has a similar behavior to the previous site 4fiv (referred to figure 4), but now for BaM + (Co, Ti)xDj

Figure 4. *Comparison between the experimental results of the Fe^{3+} distribution determined by the Rietveld method and the predictions by the model for crystallographic site 4fvi, per formula unit.*

In the site 12k (referred to figure 5) the variations of the Fe^{3+} cations quantity begin to be important starting from xDjcritical, although the behavior shows a monotonous decrease with the increment of the dopant quantity, being more evident for BaM +(Co, Sn)xDj.

Figure 5. *Comparison between the experimental results of the Fe^{3+} distribution determined by the Rietveld method and the predictions by the model for crystallographic site 12k, per formula unit.*

In the figures 6 and 7 it is noticed that when the concentration is small, with the increment of the applied field the distance between a curve and another goes decreasing, and the point of maximum magnetic susceptibility is reached.
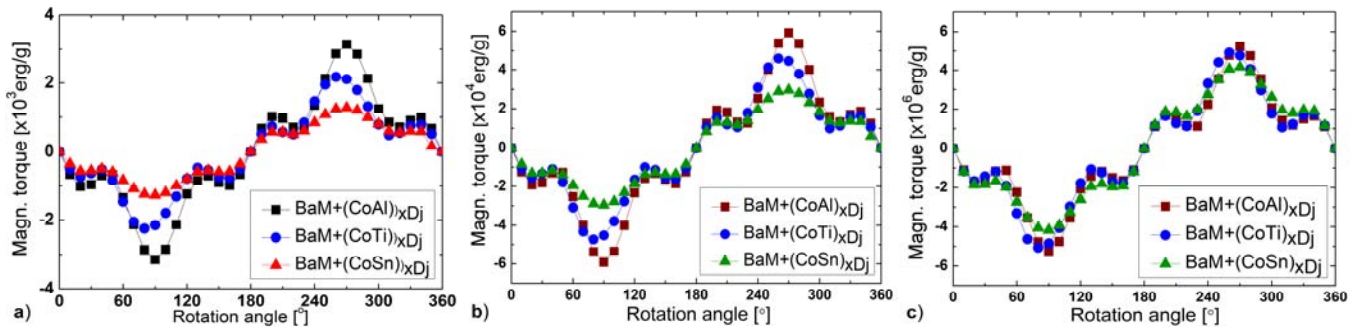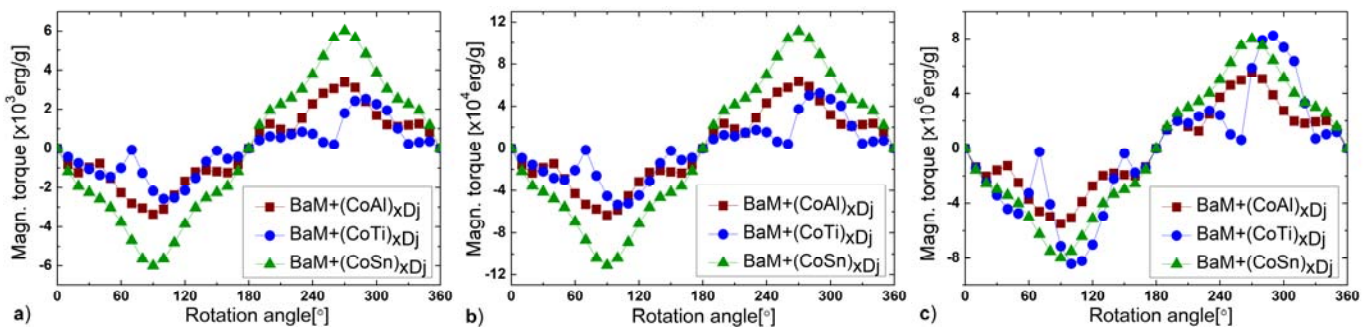
Figure 6. Magnetic torque in function of the rotation angle for the three systems, with xDj=0.1 and intensities of applied magnetic field of (a) 100 Oe, (b) 1000 Oe and (c) 9000 Oe.

A remarkable variation is observed in the magnetic torque magnitude when dopant concentration varies from 0.1 to 0.5. This statement is demonstrated by the fact that for the applied field next to the maximum magnetic susceptibility, the three curves are similar, but they are different from one concentration level to another, due to other phases contribution for systems (Co, Al) and (Co, Ti).

For xDj = 0.5 [xDj = xDj$_{critical}$ for systems (Co, Al) and (Co, Ti)], it is observed that even at high intensity of applied field (9000Oe), the distance between the curves is still appreciable, due to the other phases contribution, morphology variations and crystallites distribution inside the matrix.

Figure 7. Magnetic torque in function of the rotation angle for the three systems, with xDj = 0.5 and intensities of applied magnetic field of (a) 100 Oe, (b) 1000 Oe and (c) 9000 Oe.

In the figure 8 it is appreciated that theoretical prediction for the systems doped with (Co, Al) and (Co, Ti) appropriately reflects the dependence of MS on the dopant quantity to xDj = xDj$_{critical}$. Starting from this value, doped BaM and cobalt monoferrite contributions are presented. The experimental values for these two systems are always smaller than the theoretically predicted values, since the dopant couples preferentially go to the position 12k, and also as a result of the size and quantity of pores in these samples [4].
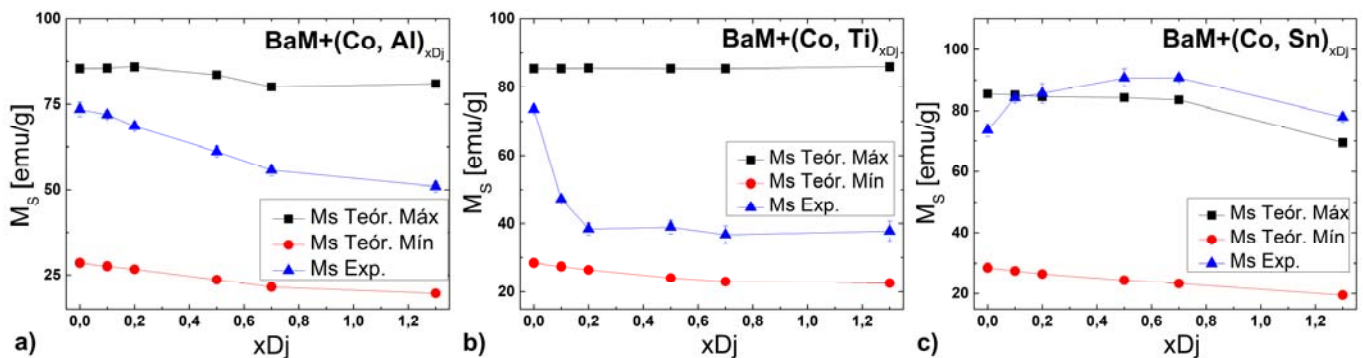
Figure 8. Experimental and theoretical saturation magnetization, in function of dopant amount per formula unit for the systems (a) BaM + (Co, Al)xDj, (b) BaM + (Co, Ti)xDj and (c) BaM + (Co, Sn)xDj.

In the figure 8 (c) it is remarkable that for the system (Co, Sn), MS tends to increase with dopant concentration, differing from the theoretically predicted values. This is because starting from a concentration value xDjcritical, the most probable process is not the formation of BaM doped with (Co, Sn) in the iron sites, but the formation of cobalt monoferrite, which is a soft magnet and it increases the magnetization for small values of xDj and tends to make constant the magnetization, starting from xDjcritical. This value coincides with the value determined by XRD.

MS depends on the contribution of each iron site to the total magnetization of the un-doped and doped samples with small dopant concentrations. Starting from values $xDj \geq xDj_{critical}$ theoretical predictions will not be of the order of the experimental characterization, because these results depend on the formed phase's type.

In the figure 9 it is important to notice that although the behavior of the theoretical and experimental densities is different, grain morphology and, consequently, the pores, only contribute to the anisotropy magnitude variation, not in the behavior. Therefore, we can infer that the dependence of this magnitude on the dopant amount is basically determined by dopant proportion in the sites 2b and 12k.
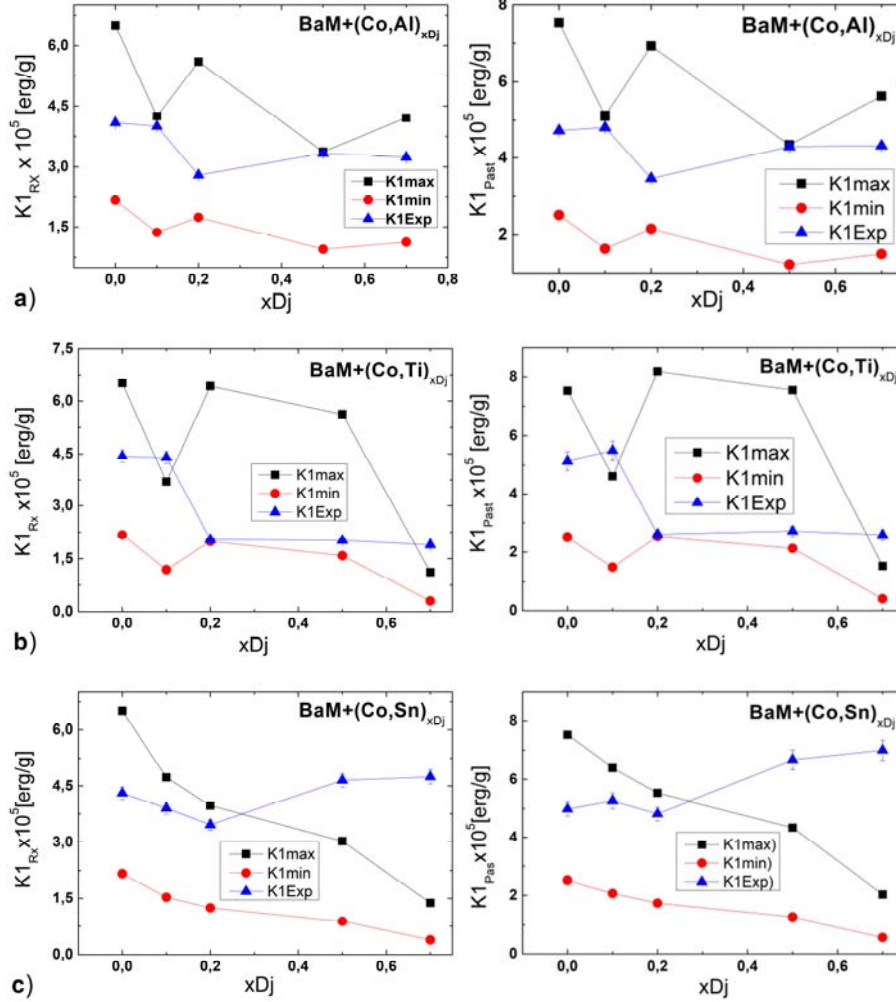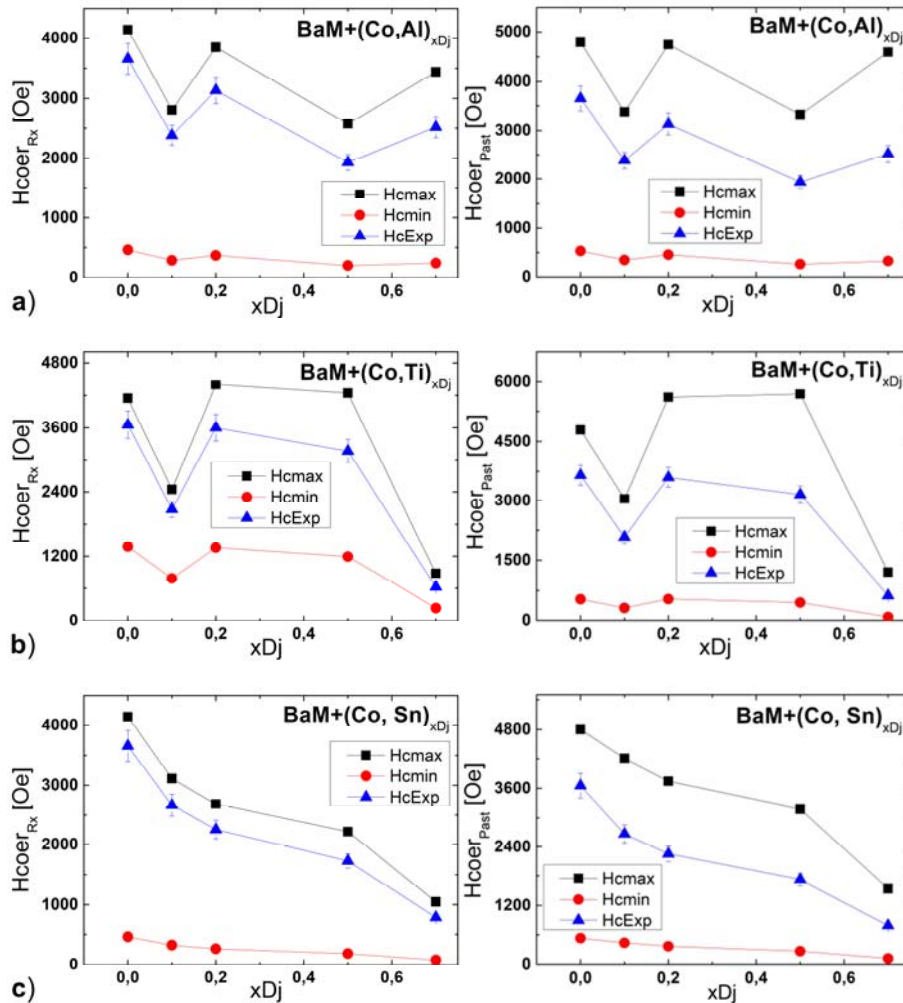

Figure 9. *Comparison between theoretical and experimental anisotropy constant K_1, considering the BaM theoretical density and density of the pill, in function of the quantity of dopant per formula unit for the systems (a) BaM + (Co, Al)xDj, (b) BaM + (Co, Ti)xDj and (c) BaM + (Co, Sn)xDj.*

For the systems (Co, Al) and (Co, Ti) there is an abrupt variation of the anisotropy with $0.1 \leq xDj \leq 0.2$, since the systems change the anisotropy type from easy axis to easy plane, which is a fact expressed in an inverse way in the predictions due to the role of the anisotropy field in this dependence.

The strains in the cell have only a secondary influence in this behavior. A very strained crystallographic cell, an excessive size of pores and the cobalt monoferrite contribution are the physical causes that do not allow to separate the magneto-crystalline anisotropy and shape anisotropy that are presented in the compounds BaM + (Co, Sn)xDj.

The deviations between the theoretical predictions and the experimental results are given by three factors: 1) The presence of other phases, microinclusions and other surface defects that contribute to the extrinsic magnetic anisotropy, 2) The strains in the structure which start increasing from the value $xDj_{critical}$ and 3) The pores inside the matrix, which tend to decrease the total magnetic anisotropy of the sample when they are big, and to increase this magnetic property when they are small.

In the figure 10 it is noticed that in all the systems the experimental values are in the predicted interval and the behavior of this parameter depends on the obtaining conditions of the samples.

***Figure 10.** Comparison between theoretical and experimental coercive field H_C, considering the BaM theoretical density and the density of the pill, in function of the quantity of dopant per formula unit for the systems (a) BaM + (Co, Al)xDj, (b) BaM + (Co, Ti)xDj and (c) BaM +(Co, Sn)xDj.*

For the substitutions with (Co2+, Sn4+) there are bigger variations of the grain size and fractions of pores, while the variations of strain coefficient are small with xDj ≤ 0.2. All these facts condition the behavior in this region of the experimental curve. Starting from this value, the fraction of pores increases in a drastic way, decreasing the coercive field intensity.

5. Conclusions

The saturation magnetization depends on the contribution of each iron site to the total magnetization of the un-doped and doped samples with small dopant concentrations and on the obtaining conditions of the compound, which significantly influence in the formed phases.

Magneto-crystalline anisotropy constant depends on the contribution of each iron site and not only of the position 2b. Its magnitude is modulated by other factors that affect the experimental results and which are not considered by the model.

There were considerable variations between the systems, in dependence of substitutes type and their distribution in the iron sites. The comparison between the theoretical predictions and the experimental results has allowed a better approach to the physical interpretation of the causes that condition the variation of the magnetic properties with the type and the concentration of two substitutes ions inside the BaM cell.

References

[1] T. Kaur, B. Kaur, B. H. Bhat, S. Kumar and A. K. Srivastava, "Effect of calcination temperature on microstructure, dielectric, magnetic and optical properties of $Ba_{0.7}La_{0.3}Fe_{11.7}Co_{0.3}O_{19}$ hexaferrites", Physica B: Condensed Matter 456, (2015) 206–212.

[2] X. Zhang, Y. Zhang, Z. Yue, J. Zhang, "Influences of sintering atmosphere on the magnetic and electrical properties of barium hexaferrites", AIP Advances 9, 085129 (2019) 1-6.

[3] R. S. Alam, M. Moradi, M. Rostami, H. Nikmanesh, R. Moayedi, Y. Bai, J. Magn. Magn. Mater. 381 (2015) 1–9.

[4] P. A. Mariño, "Estudio de la hexaferrita de bario Tipo-M dopada: predicciones y resultados experimentales", 2012, La Habana Editorial Universitaria ISBN 978-959-16-1960-0.

[5] H. Nikmanesh, S. Hoghoghifard, B. Hadi-Sichani, "Study of the structural, magnetic, and microwave absorption properties of the simultaneous substitution of several cations in the barium hexaferrite structure", Journal of Alloys and Compounds 775 (2019) 1101-1108.

[6] P. A Mariño-Castellanos, A. C. Moreno-Borges, G. Orozco-Melgar, J. A. García and E. Govea-Alcaide, "Structural and magnetic study of the Ti4+-doped barium hexaferrite ceramic samples: Theoretical and experimental results", Physica B: Condensed Matter 406 (2011) 3130–3136.

[7] P. A. Mariño, V. A. Lapshinsky, C. Pupo, J. Matilla, and A. Vega, "Obtaining and Structural Characterization of M-type Hexaferrites Doped with Two Cations in the Fe 3+ Sites" in MEPhI's Section of the Scientific Session on "Breakthrough directions of scientific research at MEPhI: Development prospects within the Strategic Academic Units", KnE Engineering, (2018), pages 328–335.

[8] L. Glasser, "Lattice energies of crystals with multiple ions: a generalized Kapustinskii equation", 1995, Inorg. Chem. 34 4935-4936.

[9] J. Matilla-Arias, E. Govea-Alcaide, P. Mariño-Castellanos, F. Rosales-Saiz "Phenomenological Model for Prediction of Cation Substitution Distribution and Some Physical Properties in Mn^{3+}-Doped Barium Hexaferrite", J Supercond Nov Magn 31 (2018) 251–256.

[10] B. B. Rath, "Kinetics of nucleation and growth processes", July 1995, Materials Science and Engineering: B 32 (3) 101-106.

[11] J. Matilla-Arias, E. Govea-Alcaide, P. Mariño-Castellanos, F. Rosales-Saiz, I. F. Machado, K. Montero-Rey, "Effects of Lanthanum on Structural and Magnetic Properties of $Sr_{1-x}La_{2x/3}Fe_{12}O_{19}$ Compounds: Theoretical and Experimental Results", JSupercondNovMagn (2019) 152-158.

[12] S. Asiri, S. Güner, A. D. Korkmaz, Md. Amir, K. M. Batoo, M. A. Almessiere, H. Gungunes, H. Sözeri, A. Baykal, " Magneto-optical properties of BaCryFe12-yO19 (0.0≤ y≤1.0) hexaferrites", Journal of Magnetism and Magnetic Materials 451 (2018) 463–472

[13] F. L Wei, H. C. Fang, C. K. Ong, C. S. Wang and Z. Yang, "Magnetic properties of $BaFe_{12-2x}Zn_xZr_xO_{19}$ particles", June 2000, J. Appl. Phys. 87 (12) 8636-8639.